Received: 5 January 2021 | Revised: 23 July 2021 | Accepted: 3 August 2021

IET Generation, Transmission & Distribution

DOI: 10.1049/gtd2.12280

The Institution of Engineering and Technology WILEY

ORIGINAL RESEARCH PAPER

Critical values of cyber parameters in a dynamic microgrid system

Lung-An Lee[1] | Chen-Ching Liu[1] | Jingyu Wang[2] | Jennifer Appiah-Kubi[1] | Kevin P. Schneider[3] | Francis K. Tuffner[3] | Dan T. Ton[4]

[1] Bradley Department of Electrical and Computer Engineering, Virginia Polytechnic Institute and State University, Blacksburg, Virginia, USA

[2] State Key Laboratory of Advanced Electromagnetic Engineering and Technology, Hubei Electric Power Security and High Efficiency Key Laboratory, and School of Electrical and Electronic Engineering, Huazhong University of Science and Technology, Wuhan, China

[3] Pacific Northwest National Laboratory, Battelle Seattle Research Center, Seattle, Washington, USA

[4] Office of Electricity Delivery and Energy Reliability, U.S. Department of Energy, Washington, District of Columbia, USA

Correspondence
Lung-An Lee, Bradley Department of Electrical and Computer Engineering, Virginia Polytechnic Institute and State University, Blacksburg, VA 24061, USA.
Email: lungan@vt.edu

Funding information
U.S. Department of Energy, Office of Electricity, and Pacific Northwest National Laboratory

Abstract

An islanded microgrid is cyber-physical system, and the control relies on the communication system significantly. Improper parameters of the cyber system can result in instability of a microgrid system. To evaluate the impact of a networked control system on control performance, a cyber model is developed to represent data acquisition periods and communication delays. Simplification of the networked control system model is proposed to enhance the computational performance, making the analytical method applicable for large-scale systems. Based on the analysis, a two-dimensional stability region of a microgrid in the space of cyber parameters can be obtained. To validate the proposed method, a microgrid control scheme is proposed for power dispatch and regulation based on the droop and proportional-integral (PI) feedback control. The analytical method is compared to the time-domain simulation, and it is shown that the stability regions are nearly identical. The critical values of cyber parameters are determined based on the analytical results. The proposed control strategy with the given cyber parameters is validated for transient stability following dynamic events. Simulation results indicate that the design of a microgrid as a cyber-physical system needs to be guided by critical values for cyber parameters to prevent system instability.

1 | INTRODUCTION

Extreme events can cause damages to power grids, leading to catastrophic outages on both transmission and distribution systems [1, 2]. To continue serving critical loads, microgrids are utilized as resiliency sources in a distribution system when the utility system becomes unavailable [3–5]. A microgrid may include one or more distributed generations (DGs), including synchronous generators, solar panels, wind turbines, and energy storage systems.

In a microgrid, a hierarchical structure is common for the control system [6, 7]. Local controllers are implemented to regulate DGs while centralized/decentralized controllers are responsible for coordination. In addition to system stability, an important issue in microgrids is the efficiency of system restoration. With limited resources, the methodology to serve maximum critical load with minimum switching operations has been proposed [8, 9]. A meshed topology is formed by multiple generators in the microgrids and a bottom-up restoration strategy is proposed [10]. Coordination of multiple microgrids with power flow solutions is proposed [11]. A power sharing control of converter-interfaced distributed energy resources (DERs) among multiple microgrids is proposed [12]. These studies indicate that a control algorithm is needed to coordinate multiple DGs in a microgrid. To control dispersed DGs, data collection via a communication system is essential. Therefore, the control system and communication system are functionally integrated as a networked control system.

Research on microgrid stability is categorized into small-signal stability, transient stability, and voltage stability [13]. A control scheme combining droop control and PI feedback control, [14–16], is validated with good performance in regulation, power dispatch, and transient stability.

This paper is concerned with the impact of the cyber system. The damage on the physical system caused by failures in the cyber system is discussed in [17]. Small-signal stability in a microgrid considering communication delays is analysed in [18, 19]. Root locus analysis shows a long delay time can drive eigenvalues to the right half-plane, causing system instability. A method for time-delay stability margin determination on power systems is proposed [20]. In [21], the status of cyber components is decided by Sequential Monte Carlo Simulation (SMCS) and their failure/repair rates. Mathematical cyber-physical models are proposed in [22, 23] to analyse the impact of cyber-contingency and transient stability in microgrids. In [24, 25], the PI controller is used for frequency control. Taking into account the communication delays, stability regions can be obtained to provide stable values of the PI parameters. In [26], a distributed secondary voltage control is proposed that incorporates communication delays via a sparse communication network. The analysis shows that system stability is dependent on time delays. In [27], the communication delay is included in the small-signal model to study system stability by eigenvalue analysis.

The performance of a cyber system, including data acquisition and exchange, is crucial to an islanded microgrid. The impact of communication delays in data exchange has been analysed using small-signal analysis based on a state-space model. However, in practice, the reporting period for data acquisition is pre-determined by design, e.g., every 2–10 seconds for data acquisition from the substations to the control centre of a power grid. This data "reporting period" of the Supervisory Control and Data Acquisition (SCADA) system is usually much longer than the communication delays that are in the order of milliseconds. The SCADA system is used for transmission and distribution grid control. Standard [28] specifies the requirements of the communication system for SCADA system. For a microgrid, however, the system has a low inertia when it is operated in an islanded mode without support from the utility system. Furthermore, Inverter-Based Resources (IBRs) can have faster responses relative to traditional synchronous generators. Therefore, a shorter cyber latency is needed to stabilize the system.

In the existing work, communication delay is the major consideration for system stability. However, the "reporting period" is typical in measurement devices and can be critical for microgrid stability as well. Furthermore, these cyber latencies are dependent. The critical value of communication delay for system stability changes under different reporting periods. The two cyber latencies need to be studied concurrently for microgrid stability. The purpose of this research is to develop an analytical method to determine the critical cyber data reporting and communication delay to ensure system stability of an islanded microgrid. A control scheme is proposed to regulate frequency and voltage at the Point of Common Coupling (PCC) node and dispatch power among DGs. A cyber model is integrated into the control system to evaluate the impact of the reporting period and communication delay.

This research deals with the use of synchronous generators to serve critical loads in an islanded microgrid when the utility system is unavailable. The control strategy can fail when the data reporting period and/or communication delay are long, leading to system instability. In this paper, an analytical method for networked control system [29] is proposed for determination of the critical values for data reporting period and communication delay in a microgrid. Small-signal analysis based on the discrete state-space model is conducted and stability regions are identified considering cyber latencies. A transformation of the transition matrix for networked control system is derived for reduction of the computational burden for calculation of the stability region. As a result, the proposed stability region method is applicable for large-scale power systems. The system stability is assessed based on the networked control method, which is validated by time-domain simulation using the non-linear dynamic model. The IEEE 13-node distribution system is used for validation of the method. The analysis provides insights into the effects of protective devices in the distribution system on the microgrid dynamics.

The main contributions of this paper include:

- An analytical method is proposed to determine the critical values of cyber parameters. The simplified method reduces the computational burden significantly, making it applicable for large-scale power systems.
- A two-dimensional stability region is obtained based on the analytical method. The stability region is critical for the design of a communication system supporting a networked control system.
- The proposed analytical method is implemented and tested with a modified IEEE 13-node test system. A networked control system is used for regulation and power dispatch of the test system. Time-domain simulations are used to validate the analytical method.

The remainder of this paper is organized as follows. Section 2 provides the microgrid control scheme. Section 3 discusses an analytical method of networked control system and the equivalent matrix for large-scale systems. Section 4 gives the state-space model of proposed control scheme. Section 5 provides the results of the analytical method and its comparison with time-domain simulation. Section 6 is concerned with validation of the system performance for scenarios of the critical reporting period and communication delay. Section 7 concludes the paper.

2 | MICROGRID CONTROL SCHEME

To maximize the restoration capability and better respond to the dynamics, based on the authors' prior work [30], DGs must share, by the same ratio, the real and reactive power output to the respective rated capacity of each DG unit. The microgrid needs to have the capability to regulate frequency and voltage to synchronize with the utility and/or other microgrids.

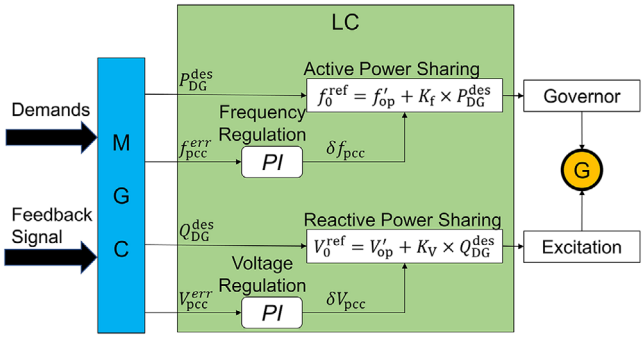

FIGURE 1 Microgrid control scheme

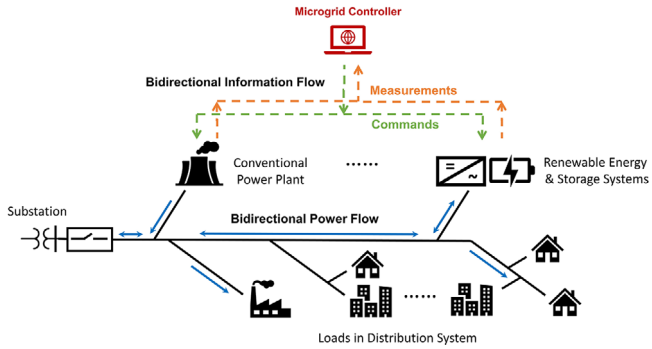

FIGURE 2 Configuration of microgrids and implementation of the proposed control scheme

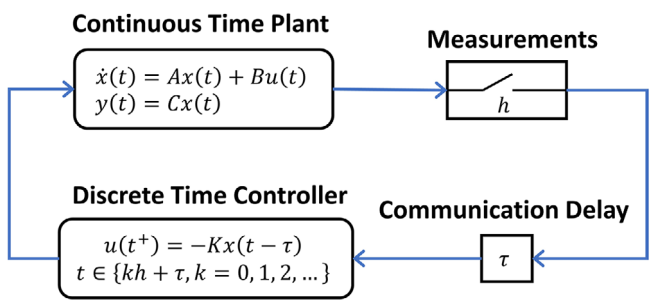

FIGURE 3 State-space model for a networked control system

A combined control scheme is proposed using droop control to share real and reactive power among DGs and PI feedback control to regulate the frequency and voltage at the PCC node.

The droop characteristics of a DG are an inversely proportional relationship between active power and frequency, K_f, or reactive power and terminal voltage, K_V. Among DGs, changing the no-load frequency and voltage references, f_0^{ref} and V_0^{ref}, will assign the desired power at the operating frequency and voltage, f_{op} and V_{op}, i.e.,

$$\begin{aligned} f_0^{ref} &= f_{op} + K_f \times P_{DG}^{des} \\ V_0^{ref} &= V_{op} + K_V \times Q_{DG}^{des} \end{aligned} \tag{1}$$

where P_{DG}^{des} and Q_{DG}^{des} are the desired active and reactive power outputs of the DG, respectively, which vary with different load conditions in real time.

To set the operating point in Equation (1), a feedback controller is designed to regulate the frequency and voltage at the PCC. Deviations from the desired frequency and voltage are acquired from the PCC and fed into the PI controllers. The new operating point is determined and Equation (1) can be rewritten to include the incremental compensations. That is,

$$\begin{aligned} f_0^{ref} &= \left(f_{op} + \delta f_{pcc}\right) + K_f \times P_{DG}^{des} = f'_{op} + K_f \times P_{DG}^{des} \\ V_0^{ref} &= \left(V_{op} + \delta V_{pcc}\right) + K_V \times Q_{DG}^{des} = V'_{op} + K_V \times Q_{DG}^{des} \end{aligned} \tag{2}$$

where δf_{pcc} and δV_{pcc} are the compensated values of frequency and voltage, and f'_{op} and V'_{op} are the adjusted operating frequency and voltage.

Figure 1 is an illustration of the control scheme. The system demand and regulation error signals are sent to the microgrid controller (MGC). After computation, MGC sends the desired power and deviations at the PCC to each local controller (LC). According to Equation (2), LCs generate references for the governor and excitation systems.

Based on the authors' prior work [30], PID control is found to be practical through a field test on a campus microgrid system. In this study, however, the overshoot is not critical (less than 5% under a 45% heavy load pick up event). Hence, the derivative control is ignored to simplify the feedback system model. The proposed control scheme is a hierarchical structure with a centralized controller, which is feasible for the general configuration of microgrids. Figure 2 shows the typical configuration of microgrids, where DGs are connected to the distribution system and serving the electrical loads. In Figure 2, the information flows are illustrated for the implementation of the proposed control scheme. Bidirectional information flows are required, measurements from sensors and commands to actuators.

3 | STATE-SPACE MODEL OF NETWORKED CONTROL SYSTEM

As a cyber-physical system, the system stability of a microgrid is impacted by the cyber latency. To determine the critical threshold for cyber latency, an analytical method is proposed in this paper.

3.1 | Networked control system

A method to analyse the Networked Control System (NCS), considering the data acquisition reporting period (h) and communication delay (τ) is developed in [29]. The state-space model with a networked control system is presented in Figure 3. A continuous state-space model is integrated with a discrete feedback controller. In a continuous state-space model, the control inputs can be fed by plant outputs simultaneously, which might not be true in practice. In a networked control system, the plant

outputs are discrete in that the sensor reports the measurements periodically at a specified time interval. Communication delay occurs while the plant and controller are exchanging data across the communication system. Note that the communication delay, τ, is a lumped value by measurement delay (plant to controller) and command delay (controller to plant). The performance of the control system can be degraded by the cyber latencies.

A continuous plant and a discrete controller are written as

$$\begin{aligned} \dot{x}(t) &= Ax(t) + Bu(t) \\ y(t) &= Cx(t) \\ u\left(t^{+}\right) &= -Kx(t-\tau),\ t \in \{kh+\tau, k=0,1,2,\ldots\} \end{aligned} \tag{3}$$

where A is state matrix, B is input matrix, C is output matrix and K is feedback matrix from state variables to input variables. The symbol h is the reporting period, k represents the k_{th} data reporting, and τ is the communication delay.

The system can be converted to an augmented closed-loop system with a transition matrix ($\tilde{\Phi}$) as Equation (4). The transition matrix is used to analyse the cyber-power system stability.

$$\begin{aligned} z((k+1)h) &= \begin{bmatrix} \Phi_{11} & \Phi_{12} \\ \Phi_{21} & 0 \end{bmatrix} z(kh) \\ &= \begin{bmatrix} \Phi - \Gamma_0(\tau) & \Gamma_1(\tau) \\ -K & 0 \end{bmatrix} z(kh) \\ &= \tilde{\Phi}(k)\, z(kh) \end{aligned} \tag{4}$$

where

$$\Phi = e^{Ah}$$

$$\Gamma_0(\tau) = \int_0^{h-\tau} e^{As} B ds$$

$$\Gamma_1(\tau) = \int_{h-\tau}^{h} e^{As} B ds$$

Stability of a discrete time linear time-invariant system is determined by the magnitude of eigenvalues of the transition matrix. The system is (asymptotically) stable if and only if all eigenvalues are located strictly inside the unit circle, i.e. the magnitude is less than 1.

3.2 | Equivalent matrix for eigenvalues

To analyse system stability, the eigenvalues of the transition matrix in Equation (4) need to be calculated. However, the computational burden is excessive, making the computation impractical for large-scale power systems. Here, a transformation of the matrix is proposed that preserves non-zero eigenvalues of the transition matrix. Based on derivation in the Appendices, the equivalent matrix for eigenvalue computation is given by

$$\tilde{\Phi}'(k) = \begin{bmatrix} e^{Ah} & \left(e^{A(2h-\tau)} - e^{A(h-\tau)}\right) A^{-1} BK \\ I_n & \left(I_n - e^{A(h-\tau)}\right) A^{-1} BK \end{bmatrix} \tag{5}$$

where A is non-singular.

With the equivalent matrix, the computational burden is reduced significantly since the complex integration of the exponential of state matrix in Equation (4) is removed.

4 | STATE-SPACE MODEL OF PROPOSED CONTROL SCHEME

The equivalent matrix is used to determine the stability regions of the networked control system. In the state-space model in Equation (3), state variables represent the dynamics of synchronous generators, excitation system (Automatic Voltage Regulator, AVR), and governor system (Turbine Governor, TG). Input variables are the reference values of AVR and TG, which are fed by the controller. The input variables include the feedback from state variables, as shown in Equation (3). The proposed controller includes two control schemes i.e. regulation and power dispatch. To compute the feedback matrix, K, it is assumed that there exists a non-singular closed-loop state matrix, $A_c = A - BK$, under continuous time linear time-invariant system.

$$\begin{aligned} \dot{x}(t) &= Ax(t) + Bu(t) \\ &= Ax(t) - BKx(t) \\ &= A_c x(t) \\ y(t) &= Cx(t) \end{aligned} \tag{6}$$

where $x(t)$ is a $n \times 1$ vector. $u(t)$ is a $m \times 1$ vector. $y(t)$ is a $p \times 1$ vector. A and A_c are $n \times n$ matrices. B is a $n \times m$ matrix. K is a $m \times n$ matrix. C is a $p \times m$ matrix.

4.1 | Regulation control in the state space

Taking frequency regulation as a control objective, the PI controller can be written as

$$\begin{aligned} \dot{q}_1(t) &= K_{\mathrm{I}}\left(f_{\mathrm{op}} - f_{\mathrm{PCC}}\right) \\ f_{\mathrm{REG}}^{ref}(t) &= q_1(t) + K_{\mathrm{P}}\left(f_{\mathrm{op}} - f_{\mathrm{PCC}}\right) \end{aligned} \tag{7}$$

where f_{REG}^{ref} is the output of PI controller, the frequency reference for regulation control. q_1 is a new state variable to represent the integral control. K_{P} and K_{I} are PI constants. f_{op} is a constant (1 p.u.) and f_{PCC} is one of the state variables.

The incremental form of Equation (7) is

$$\begin{aligned} \Delta\dot{q}_1(t) &= -K_{\mathrm{I}} \times \Delta f_{\mathrm{PCC}} \\ \Delta f_{\mathrm{REG}}^{ref}(t) &= \Delta q_1(t) - K_{\mathrm{P}} \times \Delta f_{\mathrm{PCC}} \end{aligned} \tag{8}$$

In the microgrid system, f_{PCC} is a state variable.

$$\Delta f_{\mathrm{PCC}} = R_{1\times n}^{f_{\mathrm{PCC}}} \quad \Delta x(t) = R_{1\times n}^{f_{\mathrm{PCC}}} A_c^{-1} \Delta \dot{x}(t) \tag{9}$$

where $R_{1\times n}^{f_{\mathrm{PCC}}}$ is a row vector of length n with all zeros except a 1 at the position of f_{PCC} in state variables ($R_{1\times n}^{f_{\mathrm{PCC}}} \times x(t) = f_{\mathrm{PCC}}$). Equation (8) can be written as

$$\begin{aligned}
\Delta \dot{q}_1(t) &= -K_{\mathrm{I}} \times R_{1\times n}^{f_{\mathrm{PCC}}} A_c^{-1} \Delta \dot{x}(t) \\
\Delta q_1(t) &= -K_{\mathrm{I}} \times R_{1\times n}^{f_{\mathrm{PCC}}} A_c^{-1} \Delta x(t) \\
\Delta f_{\mathrm{REG}}^{ref}(t) &= \Delta q_1(t) - K_{\mathrm{P}} \times \Delta f_{\mathrm{PCC}} \\
&= -\left(K_{\mathrm{P}} \times R_{1\times n}^{f_{\mathrm{PCC}}} + K_{\mathrm{I}} \times R_{1\times n}^{f_{\mathrm{PCC}}} A_c^{-1}\right) \Delta x(t) \\
&= -K_{\mathrm{REG}} \Delta x(t)
\end{aligned} \tag{10}$$

where K_{REG} is the feedback matrix for regulation.

4.2 | Dispatch control in the state space

Dispatch control signals are the power outputs from DGs that are output variables in the state-space model. Taking active power dispatch as an example, the droop compensation in Equation (2) can be linearized and written as

$$\begin{aligned}
f_{\mathrm{DIS}}^{ref} &= K_{\mathrm{f}} \times P_{\mathrm{DG}}^{\mathrm{des}} \\
&= K_{\mathrm{f}} \times \sum_{i}^{l} W_i P_i \\
&= K_{\mathrm{f}} \times \sum_{i}^{l} W_i R_{1\times p}^{\mathrm{P}_i} C x(t)
\end{aligned} \tag{11}$$

where f_{DIS}^{ref} is the frequency reference for dispatch control. K_{f} is the f-P droop characteristics. l is the number of DGs. W_i is the ratio of the i_{th} DG's rated capacity to the combined generation capacity, respectively. P_i is the i_{th} DG's active power which is an output variable in the state-space model. $R_{1\times p}^{\mathrm{P}_i}$ is a row vector of length p with all zeros except a one at the position of P_i in output variables ($R_{1\times p}^{\mathrm{P}_i} y(t) = R_{1\times p}^{\mathrm{P}_i} Cx(t) = P_i$).

After linearizing Equation (11), the power dispatch is written as

$$\begin{aligned}
\Delta f_{\mathrm{DIS}}^{ref}(t) &= K_{\mathrm{f}} \times \Delta P_{\mathrm{DG}}^{\mathrm{des}} \\
&= K_{\mathrm{f}} \times \sum_{i}^{l} W_i R_{1\times p}^{\mathrm{P}_i} C \Delta x(t) \\
&= -K_{\mathrm{DIS}} \Delta x(t)
\end{aligned} \tag{12}$$

where K_{DIS} is the feedback matrix for power dispatch.

4.3 | Feedback control in the state space

The feedback matrix is formed by the signals of regulation and dispatch controls. Taking frequency control as an example, the reference value of governor system is the combination of Equations (10) and (12).

$$\begin{aligned}
\Delta u_{TG}(t) &= \Delta f_{\mathrm{REG}}^{ref}(t) + \Delta f_{DIS}^{ref}(t) \\
&= -K_{\mathrm{REG}} \Delta x(t) - K_{\mathrm{DIS}} \Delta x(t) \\
&= -(K_{\mathrm{REG}} + K_{\mathrm{DIS}}) \Delta x(t) \\
&= -K_{TG} \Delta x(t)
\end{aligned} \tag{13}$$

where $\Delta u_{TG}(t)$ is the frequency reference of governor system. K_{TG} is the complete feedback matrix of frequency control.

Following the same process, the feedback matrix for voltage control can be obtained.

$$\Delta u_{AVR}(t) = -K_{AVR} \Delta x(t) \tag{14}$$

where $\Delta u_{AVR}(t)$ is the voltage reference of excitation system. K_{AVR} is the complete feedback matrix of voltage control.

The complete feedback matrix of system is written as

$$\begin{aligned}
\Delta u(t) &= \begin{bmatrix} \Delta u_{TG}(t) \\ \Delta u_{AVR}(t) \end{bmatrix} \\
&= \begin{bmatrix} -K_{TG} \\ -K_{AVR} \end{bmatrix} \Delta x(t) \\
&= -\mathrm{K}\Delta \mathrm{x}(\mathrm{t})
\end{aligned} \tag{15}$$

With the state-space model of a microgrid, the feedback matrix of proposed control scheme can be computed with Equations (7)–(15). Then, with the given state matrix A, input matrix B, and the feedback matrix K, the equivalent matrix in Equation (5) can be formed for the given reporting period and communication delay. The eigenvalues of the equivalent matrix are used to assess system stability.

4.4 | Stability region in cyber system parameters

The stability region in the two-dimensional space of cyber system parameters, h and τ, is proposed for determination of their critical values for system stability. For different pairs of the cyber parameters, the set of points forming the boundary of the (asymptotic) stability region of the microgrid system is found based on the eigenvalues. It is important to note that the dimension of the stability region is 2, irrespective of the power system size. Therefore, the proposed computational technique for the critical cyber parameters is applicable to large-scale power system models.

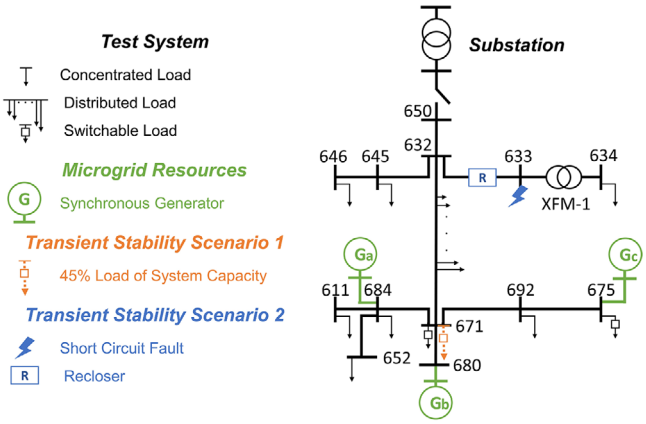

FIGURE 4 Modified IEEE 13-node test system

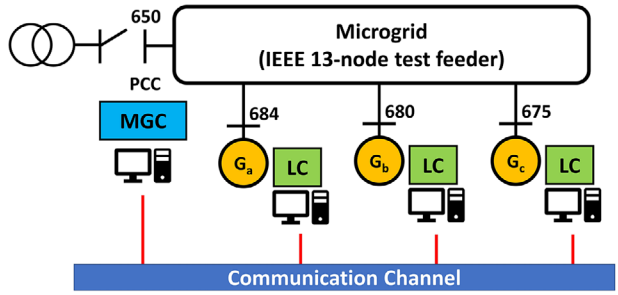

FIGURE 5 Microgrid test system with an integrated communication channel

5 | STABILITY REGION OF THE 13-NODE TEST SYSTEM

In this section, the proposed method is applied to the 13-node system. To evaluate the control performance under the influence of a cyber system, a communication link is added to the 13-node test system.

5.1 | Modified 13-node test system with cyber latency

Figure 4 shows the modified IEEE 13-node test system. Numbers in the system represent the 13 nodes. The substation circuit breaker is opened to represent an islanded microgrid in a resiliency mode. Three synchronous generators representing microgrids are located at the end of feeders. Each synchronous generator has a governor and an exciter. Their rated capacities are 2200 kVA (Ga), 3000 kVA (Gb), and 1500 kVA (Gc), respectively. A total of 6700 kVA of generation capacity serves the load of 4053 kVA. To place Ga at node 684, line 671–684 is modified from 2-phase to 3-phase. Two switches are added to the load served from nodes 671 and 675 for service restoration.

Two additional scenarios, a heavy load pick-up and a short circuit fault, are developed for the transient stability test in Section 6. An additional load at 45% of the system capacity is deployed at node 671 for the heavy load pick-up scenario. A short circuit fault is initiated at node 633, and then the recloser on Line 632–633 is set to clear the fault.

The cyber latency is modelled for the tasks of data exchange, measurements from LCs to MGC, and commands from MGC to LCs, as shown in Figure 5.

Considering that MGC and LCs can be dispersed in a wide area, cellular communication is a potential choice for the connections between MGC and LCs. At present, 4G/LTE is the most common cellular communication technology. The communication delay of 4G/LTE is a few tens of milliseconds. The benefits of the 4G/LTE technology include good performance in latency (a few tens of milliseconds) and wide availability. Furthermore, there is no need for a proprietary communication network; rather, an existing secure cellular infrastructure can be utilized for microgrid control.

A typical communication delay is much shorter than the time constants of a synchronous generator. Therefore, it should not severely impact system stability. However, with long reporting periods for data acquisition, or under a denial-of-service (DoS) cyberattack, the delay time can be prolonged.

TABLE 1 Voltage profiles in PSAT and simulink models

	PSAT (p.u.)	Simulink (p.u.)	Error (%)
Bus 684 (G1)	1.0215	1.0128	0.86
Bus 680 (G2)	1.0267	1.0163	1.02
Bus 675 (G3)	1.0220	1.0133	0.86
Bus 671	1.0201	1.0120	0.80
Bus 632	0.99969	1	0.03
Bus 633	0.99619	0.9972	0.10
Bus 634	0.9762	0.9770	0.08
Bus 650 (PCC)	0.99969	1	0.03

5.2 | Analysis by state-space model

The proposed analytical method in Section 3 is applied to the modified IEEE 13-node test system. The test system is built with the power system analysis toolbox (PSAT) [31], which only allows a balanced system model. It is assumed that the control only applies to the three-phase portion (primary feeder) of the distribution system and not the single or two-phase lateral(s) branching from the primary feeder.

For an unbalanced system, the structures of the synchronous generator, governor, and exciter remain balanced by design, so the state matrix A and input matrix B do not change. Although the unbalanced output matrix could generate three-phase output variables, the control input takes the average value to calculate the command. To validate the balanced three-phase feeder model for the control system, the balanced steady-state power flow is performed with PSAT and compared to the results in the unbalanced system in Simulink under a continuous mode. Table 1 shows the power flow results. Note that the steady-state

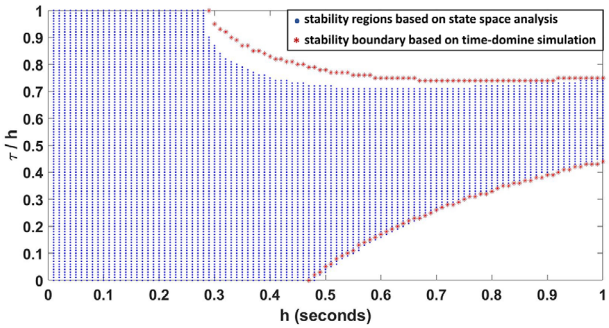

FIGURE 6 Stability regions by analytical method and time-domain simulation

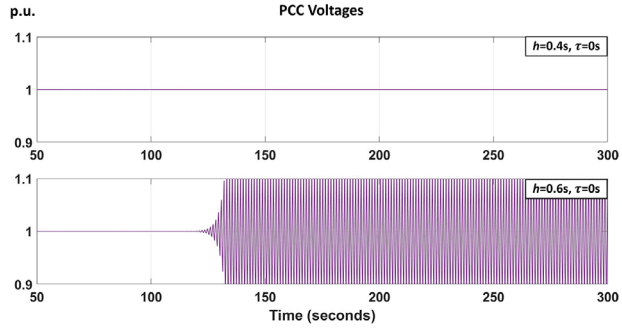

FIGURE 7 Stable and unstable system responses by time-domain simulation

operating point of the balanced model in PSAT is close to that of the unbalanced model in Simulink.

With the data acquisition reporting period and communication delay, the eigenvalues of transition matrix in Equation (4) can be computed by the equivalent matrix in Equation (5) and used to assess system stability.

For example, with 0.4-s reporting period and zero communication delay, the microgrid system is stable since the dominant eigenvalue, 0.9570, lies within the unit circle. On the other hand, with 0.6-s reporting period and zero communication delay, the system is unstable as the dominant eigenvalue, −1.2676, falls outside the unit circle.

The blue shaded area in Figure 6 is the stability region based on the state-space networked control model. The equivalent matrix, (5), is used to compute the dominant eigenvalue under the given reporting period and communication delay. Note that the stability region is a two-dimension diagram which is only associated with the two cyber parameters, i.e. reporting period and communication delay.

5.3 | Reduced computational burden

In this paper, an equivalent matrix is proposed to compute the eigenvalues of the transition matrix. The computational burden is reduced remarkably. In the modified IEEE 13-node system, the size of state matrix is 34 by 34 ($n = 34$), and input matrix is 34 by 6 ($m = 6$). The computation of eigenvalues is performed in Matlab R2018b with processor Intel(R) Core(TM) i7-10510U CPU. Using the equivalent matrix n Equation (5), the computation time is less than one minute for a total of 10201 (101 by 101) matrices in Figure 6. On the other hand, due to the integration of exponential of state matrix, the computation is much heavier by using transition matrix in Equation (4), which requires over two minutes for just one matrix.

5.4 | Validation by time-domain simulation

Time-domain simulation is performed in Simulink for the purpose of validation for the networked control method. The same models and parameters of DGs, AVRs, TGs, and PI controllers are used with the balanced system in PSAT. Various reporting periods and communication delays are applied to analyse system stability. The frequency and voltage at PCC (bus 650) are obtained. Figure 7 is the simulation results using 0.4- and 0.6-s reporting periods.

The proposed control algorithm will regulate the frequency and voltage at the PCC. The simulations start under the continuous mode to reach a stable operating point. Then, the cyber latency is added at 50 s to simulate the networked control system. With the shorter reporting period, 0.4 s, the system is regulated to 1 p.u. and the system is stable. However, with the larger reporting period, 0.6 s, the system voltage starts to oscillate at 120 s and diverges eventually, and the system becomes unstable.

To identify the critical values for the reporting period and communication delay, the stability region is obtained by the networked control method with the equivalent matrix. To validate the results, the time-domain simulation is used to find the stability boundary for the modified IEEE 13-node system. The red dotted curves in Figure 6 form the stability boundary of the microgrid system. By comparing the results from the networked control method and time-domain simulation, the differences are small. Under certain reporting periods, the maximum differences of communication delays are less than 10 ms for the lower boundary and 35 ms for the upper boundary. Note that the analytical method is based on a linearized system model, so the effect of non-linearity is not captured. In contrast, time-domain simulation is based on the non-linear dynamic model. Also, there are limitations in the governor and exciter models that are not incorporated in the linearized model. Moreover, as stated previously, the networked control system analysis is based on a balanced system, while time-domain simulation uses an unbalanced system model.

The stability region shows the cyber system performance needs to be coordinated with the physical system. Indeed, in Figure 6, when the reporting period (horizontal axis) exceeds 0.49 s, stability cannot be achieved by simply minimizing the communication delay. Based on the stability region, the communication delay needs to stay within a calculated range. In Figure 6, when the critical reporting period is 0.48 s, and the maximum communication delay is 0.3456 s (72% of the critical reporting period 0.48 s).

Considering the small errors of the state-space model, the critical threshold for communication latency in this test case is set at 0.43-s reporting period and 310-ms communication delay (10% margin).

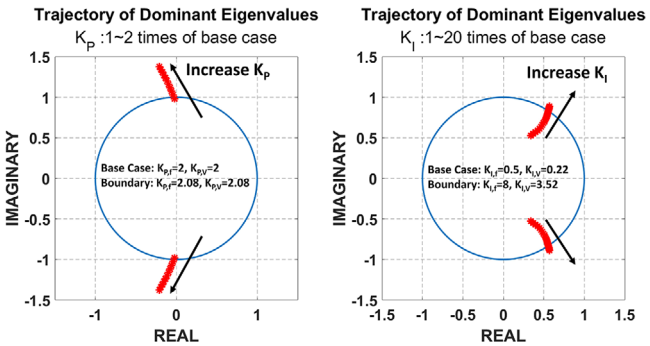

FIGURE 8 Trajectories of dominant eigenvalues as PI parameters increase

5.5 | Impact of controller parameters on stability regions

In this section, the relationship between controller gains and stability margins is analysed. Variations of the controller gains will result in a change of the two-dimensional stability region. In the proposed analytical method, the controller is involved in the feedback matrix K, which is critical in placing the eigenvalues of the equivalent matrix in Equation (5).

The stability of the transition matrix, $\tilde{\Phi}'$, is dependent on the magnitude of the dominant eigenvalue (one with the largest absolute value). In Equation (10), the PI parameters, K_P and K_I, of the proposed control method are scalar coefficients to the matrix K. Increasing the PI parameters leads to a larger magnitude of the dominant eigenvalue, reducing the stability region.

The PI parameters are designed based on the eigenvalue placement and given in the Appendices. Figure 8 shows the trajectories of the dominant eigenvalues as PI parameters increase. Since K_P is much larger then K_I in the base case, K_P dominates the elements of K and the dominant eigenvalue of $\tilde{\Phi}'$. Increasing K_P drives the dominant eigenvalues outside the unit circle quickly, leading to system instability.

Figure 9 is the stability regions with different K_P values computed by the analytical method. The red mark x is the critical thresholds of cyber latency in Section 5.4. In Figure 9(a), the base case, the operating point lies inside the stable region but is close to the boundary. This is chosen as a critical operating point with a small margin. In Figure 9(b), when the K_P increases to 1.5 times, the stability region shrinks, and the same operating point becomes unstable. With a larger K_P, the stability region shrinks further and becomes smaller as shown in Figure 9(c).

6 | MICROGRID SYSTEM PERFORMANCE UNDER CRITICAL CYBER LATENCY

In this section, the control scheme and two dynamic scenarios are tested under the critical thresholds for cyber latency determined in Section 5, i.e. $h = 0.43$ s and $\tau = 310$ ms. To implement the time-varying communication delays, a normal distribution is used for communication delays with the mean value of 310 ms and the standard deviation of 31 ms in the time-domain simulation.

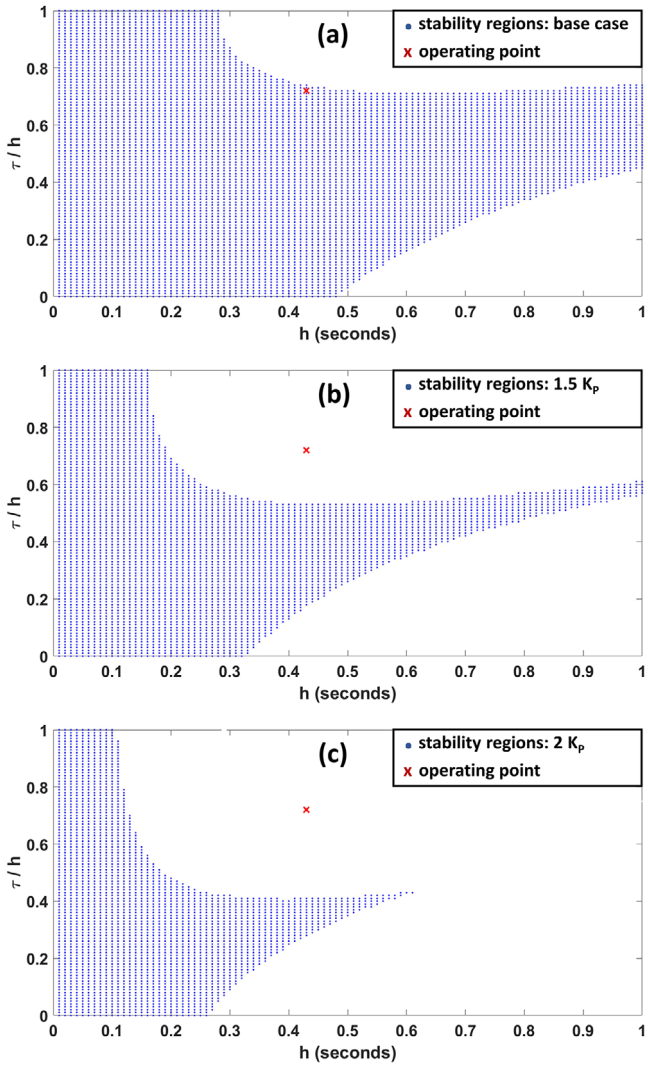

FIGURE 9 Stability regions with different K_P values

Two additional scenarios are developed for the transient stability test. In the heavy load scenario, an additional load at bus 671 is picked up for evaluation of the dynamic response. For the fault scenario, a short circuit fault is assumed to occur on the primary side of transformer XFM-1, and the fault is cleared by a recloser upstream of line 632–633.

6.1 | Restoration operation

The simulation starts with fixed loads. Then, for system restoration two switchable loads under nodes 671 and 675 are picked up at 300 and 600 s, respectively. Figures 10 and 11 show the results of regulation and power dispatch controls. Both control objectives are met under the calculated critical thresholds of cyber latency. Frequency and voltage are steered to 1 p.u. and real and reactive powers are dispatched by the same ratio of power output to the rated capacity.

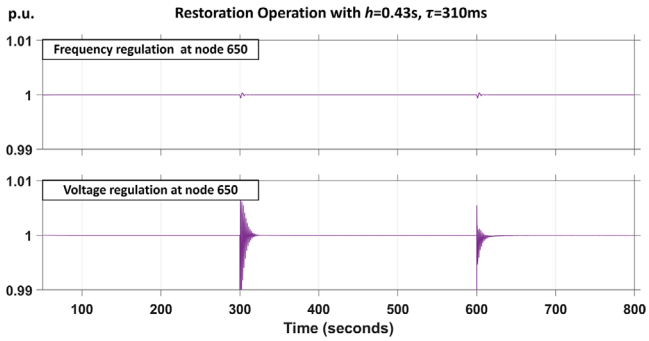

FIGURE 10 System frequency and voltage with service restoration actions

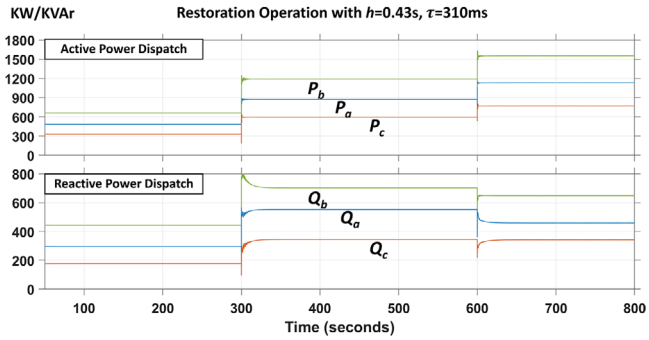

FIGURE 11 Active and reactive power dispatch with service restoration actions

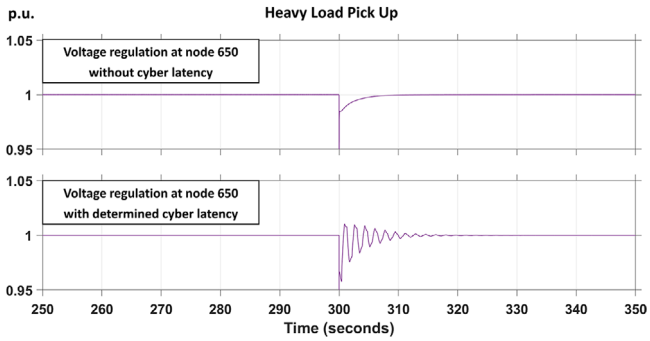

FIGURE 12 System voltage under heavy load pick up scenario

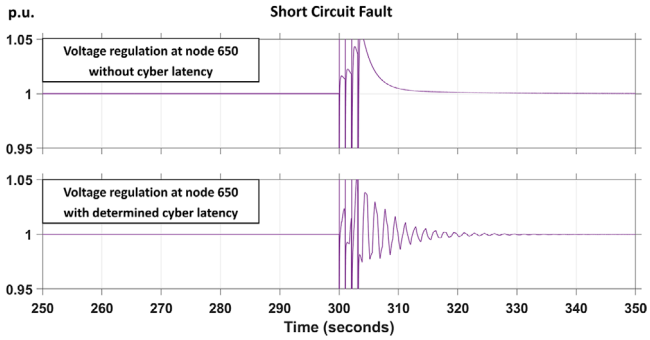

FIGURE 13 System voltage under the short circuit fault scenario

With three levels of loads, the active power outputs of the three DGs are, respectively, 483.6, 660.1, and 329.5 kW at the initial condition, 872.8, 1193.3, and 594.5 kW when node 671 is restored, and 1135.4, 1552.2, and 772.8 kW when node 675 is restored. Under all three levels, the active powers are dispatched by the same ratio to the respective rated capacity of each DG unit. Similarly, the reactive powers are dispatched by the same ratio.

6.2 | Heavy load pick up

The heavy load with 3000 kVA (0.9 lagging) load is to be picked up, representing 45% of the generation capacity. The simulation starts with fixed loads and the heavy load is picked up at 300 s. Figure 12 illustrates the voltage responses without cyber latency and under the specified cyber latency. With cyber latency, the settling time is longer, and oscillation occurs. The control commands are delayed and updated every 0.43 s. Under the specified cyber latency, the system is stable and regulated to 1 p.u. in 20 s after this transient event.

6.3 | Short circuit fault

A short circuit is assumed to occur and then it is cleared by an upstream recloser with two-fast (2 cycles) and two-delayed (5 cycles) operation settings. The simulation starts with fixed loads and the short circuit fault occurs at 300 seconds which is cleared by the recloser. Figure 13 illustrates the voltage responses without cyber latency and under the specified cyber latency. A longer settling time and oscillations are observed under the specified cyber latency. The system takes more than 30 s to settle and operate at 1 p.u. as the transients diminish.

The system performance is shown to be stable with the critical threshold for cyber latency. It is important to point out that a distribution system is normally tied to the utility system and hence dynamics are "absorbed" by the utility system. The microgrid system stability scenarios shown in this study clearly demonstrate the importance of system dynamics when the microgrid system operates in a resiliency (islanded) mode. It is also critical to study the interactions between system dynamics and the design and operation of protective devices on the feeder.

7 | CONCLUSION

The proposed analytical method is based on the networked control system model that integrates the communication and power system models. An equivalent matrix is proposed to reduce the computational burden and is feasible for large-scale power systems. Stability regions are obtained in the space of data acquisition reporting period and communication delay. This analytical method provides a systematic method to determine the stability regions and the critical threshold for cyber latency.

Time-domain simulation is used to validate the result of this analytical method.

Consequences of the cyber latency on a microgrid are observed in this study. In a realistic situation, prolonged cyber latency can occur as a result of a failure of the cyber system or malicious attacks. The future work is to implement the control scheme on a realistic distribution system and transmit data via a complete communication model. A cybersecurity monitoring system for the cyber-physical microgrid will be important.

NOMENCLATURE

K_{DIS}	Feedback matrix for power dispatch
K_{f}	$f-P$ droop characteristics
K_{I}	Integral gain
K_{P}	Proportional gain
K_{REG}	Feedback matrix for regulation
K_{V}	$V-Q$ droop characteristics
K_{AVR}	Feedback matrix to excitation system
K_{TG}	Feedback matrix to governor system
$P_{\mathrm{DG}}^{\mathrm{des}}$	Active power dispatch
$Q_{\mathrm{DG}}^{\mathrm{des}}$	Reactive power dispatch
V_0^{ref}	No-load voltage reference
V_{op}	Operating voltage
V_{op}'	Adjusted operating voltage
f_0^{ref}	No-load frequency reference
f_{DIS}^{ref}	Frequency reference for power dispatch
f_{REG}^{ref}	Frequency reference for regulation
f_{op}	Operating frequency
f_{op}'	Adjusted operating frequency
δV_{pcc}	Compensated voltage
δf_{pcc}	Compensated frequency

ACKNOWLEDGMENTS

This research was sponsored by U.S. Department of Energy Office of Electricity through the Pacific Northwest National Laboratory.

DATA AVAILABILITY STATEMENT

Research data are not shared.

ORCID

Lung-An Lee https://orcid.org/0000-0003-3010-6482

REFERENCES

1. Economic Benefits of Increasing Electric Grid Resilience to Weather Outages. https://www.energy.gov/downloads/economic-benefits-increasing-electric-grid-resilience-weather-outages (2021). Accessed January 3, 2021
2. Kwasinski, A., et al.: Hurricane Maria effects on Puerto Rico electric power infrastructure. IEEE Power Energy Technol. Syst. J. 6(1), 85–94 (2019)
3. Xu, Y., et al.: Microgrids for service restoration to critical load in a resilient distribution system. IEEE Trans. Smart Grid 9(1), 426–437 (2018)
4. Schneider, K.P., et al.: Evaluating the feasibility to use microgrids as a resiliency resource. IEEE Trans. Smart Grid 8(2), 687–696 (2017)
5. Gao, H., et al.: Resilience-oriented critical load restoration using microgrids in distribution systems. IEEE Trans. Smart Grid 7(6), 2837–2848 (2016)
6. Bidram, A., Davoudi, A.: Hierarchical structure of microgrids control system. IEEE Trans. Smart Grid 3(4), 1963–1976 (2012)
7. Wu, X., et al.: A two-layer distributed cooperative control method for islanded networked microgrid systems. IEEE Trans. Smart Grid 11(2), 942–957 (2020)
8. Li, J., et al.: Distribution system restoration with microgrids using spanning tree search. IEEE Trans. Power Syst. 29(6), 3021–3029 (2014)
9. Wang, Y., et al.: Coordinating multiple sources for service restoration to enhance resilience of distribution systems. IEEE Trans. Smart Grid 10(5), 5781–5793 (2019)
10. Feltes, J., Grande-Moran, C.: Down, but not out: A brief overview of restoration issues. IEEE Power Energy Mag. 12(1), 34–43 (2014)
11. Li, Y., et al.: Compositional power flow for networked microgrids. IEEE Power Energy Technol. Syst. J. 6(1), 81–84 (2019)
12. Shahnia, F., et al.: Primary control level of parallel distributed energy resources converters in system of multiple interconnected autonomous microgrids within self-healing networks. IET Gener. Transm. Distrib. 8(2), 203–222 (2014)
13. Majumder, R.: Some aspects of stability in microgrids. IEEE Trans. Power Syst. 28(3), 3243–3252 (2013)
14. Katiraei, F., Iravani, M.R.: Power management strategies for a microgrid with multiple distributed generation units. IEEE Trans. Power Syst. 21(4), 1821–1831 (2006)
15. Lopes, J.A.P., et al.: Defining control strategies for microgrids islanded operation. IEEE Trans. Power Syst. 21(2), 916–924 (2006)
16. Ghanbari, N., Bhattacharya, S.: Adaptive droop control method for suppressing circulating currents in DC microgrids. IEEE Open Access J. Power Energy 7, 100–110 (2020)
17. Angle, M.G., et al.: Identifying and anticipating cyberattacks that could cause physical damage to industrial control systems. IEEE Power Energy Technol. Syst. J. 6(4), 172–182 (2019)
18. Liu, S., et al.: Impact of communication delays on secondary frequency control in an islanded microgrid. IEEE Trans. Ind. Electron. 62(4), 2021–2031 (2015)
19. Ahumada, C., et al.: Secondary control strategies for frequency restoration in islanded microgrids with consideration of communication delays. IEEE Trans. Smart Grid 7(3), 1430–1441 (2016)
20. Dong, C., et al.: Effective method to determine time-delay stability margin and its application to power systems. IET Gener. Transm. Distrib. 11(7), 1661–1670 (2017)
21. Wang, C., et al.: Impacts of cyber system on microgrid operational reliability. IEEE Trans. Smart Grid 10(1), 105–115 (2019)
22. Xin, S., et al.: Cyber-physical modeling and cyber-contingency assessment of hierarchical control systems. IEEE Trans. Smart Grid 6(5), 2375–2385 (2015)
23. Farraj, A., et al.: A cyber-physical control framework for transient stability in smart grids. IEEE Trans. Smart Grid 9(2), 1205–1215 (2018)
24. Veronica, A.J.S.J., et al.: Robust PI controller design for frequency stabilisation in a hybrid microgrid system considering parameter uncertainties and communication time delay. IET Gener. Transm. Distrib. 13(14), 3048–3056 (2019)
25. Gündüz, H., et al.: Comprehensive gain and phase margins based stability analysis of microgrid frequency control system with constant communication time delays. IET Gener. Transm. Distrib. 11(3), 719–729 (2017)
26. Lai, J., et al.: Distributed secondary voltage control for autonomous microgrids under additive measurement noises and time delays. IET Gener. Transm. Distrib. 13(14), 2976–2985 (2019)

27. Liang, H., et al.: Stability enhancement of decentralized inverter control through wireless communications in microgrids. IEEE Trans. Smart Grid 4(1), 321–331 (2013)
28. IEEE Standard for SCADA and Automation Systems. IEEE Std C37.1-2007 (Revision of IEEE Std C37.1-1994). pp. 1–143. IEEE, Piscataway, NJ (2008)
29. Zhang, W., et al.: Stability of networked control systems. IEEE Control Syst. Mag. 21(1), 84–99 (2001)
30. Lee, L.A., et al.: Dynamics and control of microgrids as a resiliency source. Int. Trans. Electr. Energy Syst. 30(11), e12610 (2020)
31. Milano, F.: An open source power system analysis toolbox. In: 2006 IEEE Power Engineering Society General Meeting. Montreal, QC (2006)

How to cite this article: Lee, L.-A., et al.: Critical values of cyber parameters in a dynamic microgrid system. IET Gener. Transm. Distrib. 2022;16:99–109. https://doi.org/10.1049/gtd2.12280.

APPENDICES

Equivalent matrix of networked control system

Assume the state matrix $\mathcal{A}$ is non-singular, and λ is non-zero eigenvalue of the transition matrix in Equation (4). Then, the following equation is satisfied.

$$det\left[\tilde{\Phi}(k)-\lambda I_{n+m}\right]=det\begin{bmatrix}\Phi_{11}-\lambda I_n & \Phi_{12}\\ \Phi_{21} & -\lambda I_m\end{bmatrix}=0 \tag{A.1}$$

Since λ is non-zero eigenvalue, $-\lambda I_m$ is invertible. Hence,

$$\begin{aligned}&det\begin{bmatrix}\Phi_{11}-\lambda I_n & \Phi_{12}\\ \Phi_{21} & -\lambda I_m\end{bmatrix}\\ &=det\,(-\lambda I_m)\,det\left[(\Phi_{11}-\lambda I_n)-\Phi_{12}(-\lambda I_m)^{-1}\Phi_{21}\right]\\ &=0\end{aligned} \tag{A.2}$$

Since $det(-\lambda I_m)$ is non-zero,

$$\begin{aligned}&det\left[(\Phi_{11}-\lambda I_n)-\Phi_{12}(-\lambda I_m)^{-1}\Phi_{21}\right]\\ &=det\left(\Phi_{11}+\frac{1}{\lambda}\Phi_{12}\Phi_{21}-\lambda I_n\right)\\ &=0\end{aligned} \tag{A.3}$$

Multiplying on both side of (non-zero term, $det(\lambda\mathcal{A})$, it is obtained that

$$det\left(\lambda^2\mathcal{A}-\lambda\mathcal{A}\Phi_{11}-\mathcal{A}\Phi_{12}\Phi_{21}\right)=0 \tag{A.4}$$

To eliminate the integration of exponential of state matrix, the following identity is used.

$$X\left(\int_0^T e^{Xt}dt\right)+I=e^{XT} \tag{A.5}$$

Then, Equation (A.4) can be transformed. That is,

$$\begin{aligned}&det\left(\lambda^2\mathcal{A}-\lambda\mathcal{A}\Phi_{11}-\mathcal{A}\Phi_{12}\Phi_{21}\right)\\ &=det\begin{pmatrix}\lambda^2\mathcal{A}\\ -\lambda\left[\mathcal{A}e^{\mathcal{A}b}-\mathcal{A}\int_0^{b-\tau}e^{\mathcal{A}s}dsBK\right]\\ +\mathcal{A}\int_{b-\tau}^{b}e^{\mathcal{A}s}dsBK\end{pmatrix}\\ &=det\begin{pmatrix}\mathcal{A}\lambda^2\\ -\lambda\mathcal{A}e^{\mathcal{A}b}+\lambda\left[\mathcal{A}\int_0^{b-\tau}e^{\mathcal{A}s}ds+I_n\right]BK-\lambda BK\\ +\left[\mathcal{A}\int_0^{b}e^{\mathcal{A}s}ds+I_n\right]BK-\left[\mathcal{A}\int_0^{b-\tau}e^{\mathcal{A}s}ds+I_n\right]BK\end{pmatrix}\\ &=det\begin{pmatrix}\mathcal{A}\lambda^2\\ +\left(e^{\mathcal{A}(b-\tau)}BK-BK-\mathcal{A}e^{\mathcal{A}b}\right)\lambda\\ +\left(e^{\mathcal{A}b}-e^{\mathcal{A}(b-\tau)}\right)BK\end{pmatrix}\\ &=det\,(\mathcal{A})\times det\begin{pmatrix}I_n\lambda^2\\ +\mathcal{A}^{-1}\left(e^{\mathcal{A}(b-\tau)}BK-BK-\mathcal{A}e^{\mathcal{A}b}\right)\lambda\\ +\mathcal{A}^{-1}\left(e^{\mathcal{A}b}-e^{\mathcal{A}(b-\tau)}\right)BK\end{pmatrix}\\ &=0\end{aligned} \tag{A.6}$$

Since $det(\mathcal{A})\neq 0$, and $\mathcal{A}^{-1}$, $e^{\mathcal{A}b}$, $e^{\mathcal{A}(b-\tau)}$ are commutative.

$$\begin{aligned}&det\begin{pmatrix}I_n\lambda^2\\ +\mathcal{A}^{-1}\left(e^{\mathcal{A}(b-\tau)}BK-BK-\mathcal{A}e^{\mathcal{A}b}\right)\lambda\\ +\mathcal{A}^{-1}\left(e^{\mathcal{A}b}-e^{\mathcal{A}(b-\tau)}\right)BK\end{pmatrix}\\ &=det\begin{bmatrix}e^{\mathcal{A}b}-\lambda I_n & \left(e^{\mathcal{A}(2b-\tau)}-e^{\mathcal{A}(b-\tau)}\right)\mathcal{A}^{-1}BK\\ I_n & \left(I_n-e^{\mathcal{A}(b-\tau)}\right)\mathcal{A}^{-1}BK-\lambda I_n\end{bmatrix}\\ &=0\end{aligned} \tag{A.7}$$

Therefore, λ is non-zero eigenvalue of the equivalent matrix given by

$$\tilde{\Phi}'(k)=\begin{bmatrix}e^{\mathcal{A}b} & \left(e^{\mathcal{A}(2b-\tau)}-e^{\mathcal{A}(b-\tau)}\right)\mathcal{A}^{-1}BK\\ I_n & \left(I_n-e^{\mathcal{A}(b-\tau)}\right)\mathcal{A}^{-1}BK\end{bmatrix} \tag{A.8}$$

State-space model and controller parameters

Matrices of the state-space model are given via the following link.

https://data.mendeley.com/datasets/k47zjr5w9z/1

The PI parameters of the base case are given in Table A.1.

TABLE A.1 PI parameters of base case

	Proportional gain K_P	Integral gain K_I
Frequency control	2	0.22
Voltage control	2	0.5